Author's Accepted Manuscript

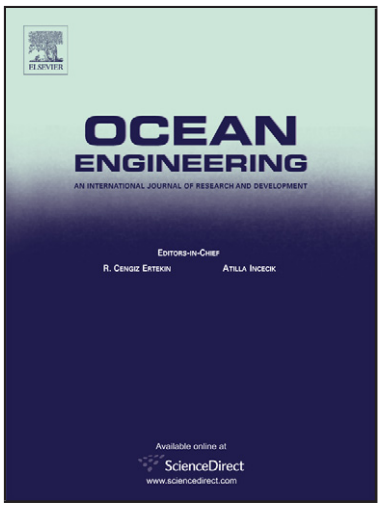

An estimate of Atlantic Ocean Thermal Energy Conversion (OTEC) resources

Gérard C. Nihous

PII: S0029-8018(07)00164-3
DOI: doi:10.1016/j.oceaneng.2007.06.004
Reference: OE 1392

To appear in: *Ocean Engineering*

www.elsevier.com/locate/oceaneng

Received date: 31 March 2007
Accepted date: 27 June 2007

Cite this article as: Gérard C. Nihous, An estimate of Atlantic Ocean Thermal Energy Conversion (OTEC) resources, *Ocean Engineering* (2007), doi:10.1016/j.oceaneng.2007.06.004

AN ESTIMATE OF ATLANTIC OCEAN THERMAL ENERGY CONVERSION (OTEC) RESOURCES

Gérard C. Nihous*

Associate Researcher

Hawaii Natural Energy Institute, University of Hawaii,

1680 East-West Road, POST 109, Honolulu, HI 96822, U.S.A.

Abstract

An interhemispheric box model of the Atlantic thermohaline circulation (THC) is modified by replacing the tropical box with two vertically-resolved sub-domains. Seawater flows from large-scale ocean thermal energy conversion (OTEC) are allowed in one of the tropical sub-domains. Under present conditions and standardized OTEC operations, steady-state net power production density would reach a maximum of about 80 kW/km^2 (corresponding to 1.8 TW) with a cold seawater withdrawal per unit area of about 14 m/yr. This maximum reflects the impact of large OTEC flows on the oceanic thermal structure, although the THC would not be significantly affected. It is larger than a recently suggested worldwide value of the order of 30 kW/km^2 because of the relative strength of the Atlantic THC. Under asymmetric high-latitude warming scenarios potentially representative of current climatic trends, a substantial weakening or a reversal of the THC are possible. In the former case, recoverable OTEC resources could practically vanish. In the latter case, the emergence of a

* Corresponding author; phone: +1-808-956-2338; fax: +1-808-956-2336; e-mail: nihous@hawaii.edu

stronger reverse THC eventually could boost OTEC resources. Such events are hypothetical and would unfold over centuries, but the mere possibility of their occurrence challenges the accepted notion that OTEC resources are forever renewable.

Keywords: ocean thermal energy conversion; global warming; Atlantic thermohaline circulation

Introduction

Ocean thermal energy conversion was formulated long ago as a way to recover some of the solar energy stored in the upper mixed layer of tropical oceans (d'Arsonval, 1881; Claude, 1930). The principle is simple and involves the extraction of mechanical work in a Rankine cycle operated between warm surface seawater and deep cold seawater. One challenge for this classical steam engine is a low thermodynamic efficiency of the order of 3%. Hence, OTEC electricity generation would require very large seawater flow rates of the order of several cubic meters per second per megawatt. This fact and other engineering difficulties typical of the offshore environment have hampered the development of OTEC. Yet, many advocates have maintained that the technology eventually will become attractive when concerns for the security of energy supplies and increases in the cost of primary energy reach critical levels (Zener, 1973; Zener, 1977; Penney and Bharathan, 1987; Penney and Daniel, 1989; Johnson, 1992; Avery and Wu, 1994; Vega, 1995; Masutani and Takahashi, 2000).

The theoretical question of the size of the OTEC resource was recently investigated after a literature survey yielded a wide range of estimates, from 10 to 1000 TW, either based on the amount of solar radiation absorbed by tropical oceans, or given without details (Nihous,

2005; Nihous, 2007). A one-dimensional analysis of OTEC operations under moderately conservative standardized conditions was conducted. Because of the potential interaction between OTEC seawater flows and the thermal structure of the water column, it was shown that OTEC resources might not exceed a few terawatts. This still represents an enormous amount of electrical power, of the order of today's installed generating capacity, but it falls short of previous estimates.

A precise evaluation of OTEC resources ultimately is warranted, for example with Ocean General Circulation Models (OGCMs), but it would require considerable analytical and computational efforts. In fact, such a task may well appear premature in the absence of near-term plans to develop OTEC on a massive scale. Yet, the simple one-dimensional analysis revealed basic points that raise further questions. It suggested that interactions between OTEC flows and the thermal structure of the tropical water column reach a critical level when the withdrawal of deep cold seawater for OTEC operations is of the same order as the upward flow of polar water (Nihous, 2005; Nihous, 2007). Although a background upwelling is an oversimplification acceptable in a one-dimensional context, it conceptually belongs to a larger global circulation – the thermohaline circulation. Good descriptions of our current understanding of the THC are available (Rahmstorf, 2006). While global ocean currents are driven by wind forcing as well as by density differences, the terminology THC should specifically refer to a circulation sustained by the effect of imbalances in temperatures and salinities on density. The stability of the Atlantic THC has been the object of much debate from the pioneering work of Stommel (1961) to present-day investigations, especially in light of a potentially strong coupling between THC and global climate (Broecker, 1997; Stocker and Schmittner, 1997; Marotzke, 2000). In a recent intercomparison experiment, various Earth Models of Intermediate Complexity (EMICs) calculated the hysteresis

response of the THC to slow changes of the North Atlantic freshwater input (Rahmstorf *et al.*, 2005). This behavior is typical of systems with multiple stable equilibrium states. For given perturbations of the atmospheric radiative forcing, Stocker and Schmittner (1997) also demonstrated the importance of rates of change. Using a two-dimensional idealized ocean, Lucarini *et al.* (2005) further explored the impact of transient changes of different time scales on THC predictions, as well as the effect of North-South forcing asymmetry.

Recent analyses based on multiple-box models have examined the possible effect of global warming on the Atlantic THC (Lucarini and Stone, 2005a; Lucarini and Stone, 2005b). The simple modeling architecture of these studies, as opposed to OGCM-based work, allows extensive parametric variations of both spatial and temporal patterns of forcing. It also presents an immediate opportunity to develop a comprehensive framework of the possible interplay between large OTEC operations and the Atlantic THC in a globally warming environment. Details about this modeling effort are given in the next Section, before results are presented and discussed further.

Model Description

The representation of the thermohaline circulation adopted here is based on the 3-box interhemispheric model of Lucarini and Stone (2005a). The ocean depth h is assumed to be constant. Two boxes account for northern and southern high latitudes, with indices N and S respectively, and the third box is the intertropical region. By choosing a latitude cutoff of 30 degrees and a uniform longitudinal width of 60 degrees to approximately define the Atlantic Ocean, the tropical box is twice as large as either high-latitude one.

Because OTEC is by definition dependent on the thermal structure of the oceanic water column, well-mixed boxes are useless in assessing OTEC resources. On the other hand, a map of temperature differences between the surface mixed layer and a typical OTEC cold seawater intake depth of the order of 1000 m shows that only about half of the Atlantic intertropical region is suitable for this technology (Nihous, 2007). The occurrence of cold currents and upwellings along much of the African West coast is responsible for this reduction in the Atlantic thermal resource. The modeling strategy adopted here is to replace the large tropical well-mixed box by two equal sub-domains where both temperature and salinity are vertically resolved, except in surface mixed layers of thickness h_m. The overall model geometry therefore consists of two boxes and two sub-domains of equal areas A and volumes V.

Variables of interest in the high-latitude boxes are the temperatures T_N and T_S, as well as the salinities S_N and S_S which are functions of time t. The two tropical sub-domains are distinguished by indices 1 and 2, respectively, and OTEC operations are allowed in the former. The water-column temperature and salinity profiles $\theta_1(t, z)$, $\theta_2(t, z)$, $s_1(t, z)$ and $s_2(t, z)$, as well as the time-dependent mixed-layer variables T_1, T_2, S_1 and S_2 also must be determined. The vertical coordinate z is measured upward from the seafloor.

All boxes and sub-domains are connected by the THC of strength $\widetilde{q}$, with a direct flow between the two high-latitude boxes through a 'conduit' of negligible mass (as, for example, in intense deep Western boundary currents). In our representation, water from the downstream polar[1] box upwells through the two tropical sub-domains before flowing out of the tropical mixed layers into the other (upstream) polar box. This closed circulation is

illustrated in Figure 1 for the present-day THC, where northern water sinks and flows into the southern region. The convention adopted for this THC configuration is $\widetilde{q} \geq 0$. The background upwelling rate in the tropical water columns simply is $w = |\widetilde{q}|/(2A)$.

Calling $\widetilde{H}_i$ and $\widetilde{F}_i$ the algebraic heat and freshwater fluxes from the atmosphere to the ocean, for i = N, S, 1 and 2, heat and mass balances in the corresponding well-mixed boxes yield the following evolution equations:

$$\frac{dT_N}{dt} = \begin{cases} \frac{\widetilde{q}}{V}\left(\frac{T_1+T_2}{2} - T_N\right) + \frac{\widetilde{H}_N}{\rho_0 c_{p0} V} & \widetilde{q} \geq 0 \\ \frac{\widetilde{q}}{V}(T_N - T_S) + \frac{\widetilde{H}_N}{\rho_0 c_{p0} V} & \widetilde{q} < 0 \end{cases} \tag{1}$$

$$\frac{dT_S}{dt} = \begin{cases} \frac{\widetilde{q}}{V}(T_N - T_S) + \frac{\widetilde{H}_S}{\rho_0 c_{p0} V} & \widetilde{q} \geq 0 \\ \frac{\widetilde{q}}{V}\left(T_S - \frac{T_1+T_2}{2}\right) + \frac{\widetilde{H}_S}{\rho_0 c_{p0} V} & \widetilde{q} < 0 \end{cases} \tag{2}$$

$$\frac{dT_i}{dt} = \frac{\widetilde{H}_i}{\rho_0 c_{p0} A h_m} - \frac{K}{h_m}\frac{\partial \theta_i}{\partial z}\bigg|_{z=h-h_m} \qquad \text{i} = 1, 2 \tag{3}$$

$$\frac{dS_N}{dt} = \begin{cases} \frac{\widetilde{q}}{V}\left(\frac{S_1+S_2}{2} - S_N\right) - \frac{\widetilde{F}_N}{V} S_N & \widetilde{q} \geq 0 \\ \frac{\widetilde{q}}{V}(S_N - S_S) - \frac{\widetilde{F}_N}{V} S_N & \widetilde{q} < 0 \end{cases} \tag{4}$$

[1] 'Polar' may be used interchangeably with 'high-latitude' in the context of this model

$$\frac{dS_S}{dt} = \begin{cases} \frac{\widetilde{q}}{V}(S_N - S_S) - \frac{\widetilde{F}_S}{V}S_S & \widetilde{q} \geq 0 \\ \frac{\widetilde{q}}{V}(S_S - \frac{S_1 + S_2}{2}) - \frac{\widetilde{F}_S}{V}S_S & \widetilde{q} < 0 \end{cases} \tag{5}$$

$$\frac{dS_i}{dt} = -\frac{\widetilde{F}_i}{Ah_m}S_i - \frac{K}{h_m}\frac{\partial s_i}{\partial z}\Big|_{z=h-h_m} \qquad \text{i = 1, 2} \tag{6}$$

ρ_0 and c_{p0} are some reference seawater density and specific heat, respectively. When density has to be specified more precisely, a first-order expansion as a function of temperature and salinity is performed using average thermal and haline expansion coefficients α and β. K is a vertical turbulent diffusion coefficient in the tropical water columns below the corresponding mixed layers. In this simple model, K is a constant adjusted to specify an initial steady-state temperature profile. A fundamental relationship which further couples the above equations is the assumed proportionality of the THC strength on the seawater density difference between polar boxes (Rooth, 1982). It may be expressed as:

$$\widetilde{q} = kV[\alpha(T_S - T_N) + \beta(S_N - S_S)] \tag{7}$$

where k is a hydraulic constant. Today's THC is positive and predominantly driven by salinity, since $T_S < T_N$. The two tropical atmospheric freshwater fluxes are assumed to be equal, and if global water mass conservation is approximately expressed in terms of volumes, the following identities are obtained:

$$\widetilde{F}_1 = \widetilde{F}_2 = -\frac{(\widetilde{F}_N + \widetilde{F}_S)}{2} \tag{8}$$

Next, partial differential equations must be specified for temperature and salinity in the advective-diffusive tropical water columns in order to determine the diffusive fluxes in Equations (3) and (6). In the tropical half-domain where OTEC operations are not suitable, vertical advection is the same throughout the water column, with an upwelling rate w. Where large-scale OTEC operations are possible, however, the water column in a 1-D model must be partitioned into three distinct layers (Nihous, 2005; Nihous, 2007): from the seafloor to the OTEC cold seawater intake, $0 < z < z_{cw}$, the background advection rate is not affected; between the cold seawater intake and the mixed-effluent discharge, $z_{cw} < z < z_{mix}$, the net advection rate becomes w- Q_{cw}/A, where Q_{cw} is the OTEC cold seawater flow rate; finally, from the mixed-effluent discharge to the bottom of the mixed layer, $z_{mix} < z < h - h_m$, the net advection rate is $w + \gamma Q_{cw}/A$, where γ is the ratio of the OTEC warm seawater flow rate over Q_{cw}. The following evolution equations are thus obtained:

$$\begin{cases} \dfrac{\partial \theta_i}{\partial t} = K \dfrac{\partial^2 \theta_i}{\partial z^2} - w \dfrac{\partial \theta_i}{\partial z} \\ \dfrac{\partial s_i}{\partial t} = K \dfrac{\partial^2 s_i}{\partial z^2} - w \dfrac{\partial s_i}{\partial z} \end{cases} \quad \text{i = 1: } 0 < z < z_{cw}\text{; i = 2: } 0 < z < h - h_m, \tag{9}$$

$$\begin{cases} \dfrac{\partial \theta_1}{\partial t} = K \dfrac{\partial^2 \theta_1}{\partial z^2} - (w - \dfrac{Q_{cw}}{A}) \dfrac{\partial \theta_1}{\partial z} \\ \dfrac{\partial s_1}{\partial t} = K \dfrac{\partial^2 s_1}{\partial z^2} - (w - \dfrac{Q_{cw}}{A}) \dfrac{\partial s_1}{\partial z} \end{cases} \quad \text{i = 1: } z_{cw} < z < z_{mix}, \tag{10}$$

$$\begin{cases} \dfrac{\partial \theta_1}{\partial t} = K \dfrac{\partial^2 \theta_1}{\partial z^2} - (w + \dfrac{\gamma Q_{cw}}{A}) \dfrac{\partial \theta_1}{\partial z} \\ \\ \dfrac{\partial s_1}{\partial t} = K \dfrac{\partial^2 s_1}{\partial z^2} - (w + \dfrac{\gamma Q_{cw}}{A}) \dfrac{\partial s_1}{\partial z} \end{cases} \qquad \text{i} = 1: z_{mix} < z < h - h_m, \tag{11}$$

In both tropical water columns, i = 1, 2, similar bottom flux and top continuity conditions apply:

$$\begin{cases} -K \dfrac{\partial \theta_i}{\partial z}(t,0) + w\theta_i(t,0) = wT_S, \widetilde{q} \geq 0 \quad (wT_N, \widetilde{q} < 0) \\ \\ -K \dfrac{\partial s_i}{\partial z}(t,0) + ws_i(t,0) = wS_S, \widetilde{q} \geq 0 \quad (wS_N, \widetilde{q} < 0) \end{cases} \tag{12}$$

$$\begin{cases} \theta_i(t, h - h_m) = T_i \\ \\ s_i(t, h - h_m) = S_i \end{cases} \tag{13}$$

The initial boundary value problems in the OTEC tropical sub-domain are further defined by imposing temperature and salinity continuity conditions at $z = z_{cw}$ and $z = z_{mix}$. The values $\theta_1(t, z_{cw})$, $s_1(t, z_{cw})$, $\theta_1(t, z_{mix})$, and $s_1(t, z_{mix})$ remain unknown, however. It can be shown that expressing flux discontinuities from the OTEC sink at z_{cw} results in continuity conditions for the temperature and salinity gradients (Nihous, 2007). Known flux discontinuities from the OTEC mixed-effluent discharge at z_{mix} provide the necessary equations to close the problem.

Finally, an uncoupled parametrization of the heat and freshwater fluxes from the atmosphere to the ocean is adopted as outlined in Lucarini and Stone (2005a). The values $\widetilde{F}_N$ and $\widetilde{F}_S$ are

given and all heat processes for i = N, S, 1 and 2 are formalized as relaxation laws of the form:

$$\widetilde{H}_i = \rho_0 c_{p0} V \lambda (\tau_i - T_i) \tag{14}$$

A more elaborate approach is possible where coupling between atmosphere and ocean is explicit, and specific processes related to the transport of sensible and latent heat as well as radiative forcing are expressed separately (Lucarini and Stone, 2005b). In this case, the freshwater fluxes $\widetilde{F}_N$ and $\widetilde{F}_S$ are determined prognostically. Any influx from melting land-ice sheets also would affect global water mass conservation and necessitate a modification of Equation (8). This process, however, is difficult to define and was not explored by Lucarini and Stone (2005b) even though "the future evolution of the Atlantic THC is probably closely tied to the fate of the Greenland ice sheet (Rahmstorf, 2006)."

The amount of OTEC power corresponding to the seawater temperatures calculated in the OTEC tropical subdomain must be determined. Typically, a working fluid in a closed loop generates OTEC power in a Rankine cycle. The working fluid evaporates in an evaporator, flows through a turbine where mechanical work is generated, condenses in a condenser and is recirculated by a small feed pump. Large seawater pumps supply the heat exchangers (evaporator and condenser) with either warm surface seawater or deep cold seawater. Process temperatures are similar to those found in the refrigeration industry, so that refrigerants including ammonia are OTEC working fluids of choice. The optimum temperature drop across the turbine is only about half of the seawater temperature difference $T_1(t) - \theta_1(t, z_{cw})$ since some of the ocean thermal resource is also used in the heat exchangers (Johnson,

1992). It can be shown that the thermodynamic efficiency of this ideal Rankine cycle is close to $0.5\{T_1(t) - \theta_1(t, z_{cw})\}/\{273.15 + T_1(t)\}$. In the standard OTEC process proposed by Nihous (2005), the seawater flowrate ratio γ is equal to 2 (values larger than one reflect the greater accessibility of surface water in design optimizations). The minimum temperature separation (pinch) which must be maintained between seawater and working fluid to drive heat flow in the heat exchangers is assumed to be $\{T_1(t) - \theta_1(t, z_{cw})\}/16$. The large heat loads in the evaporator and condenser are then estimated by neglecting OTEC power in an overall heat-and-mass balance. Calling ε_{tg} the turbogenerator efficiency, which accounts for irreversible losses through the thermodynamic cycle as well as during the conversion of mechanical work to electricity, the gross electrical power produced by the generator is the product of ε_{tg} times the ideal cycle efficiency times the evaporator heat load. Omitting further details, the net OTEC electrical power P_{net} is written as:

$$P_{net} = \frac{Q_{cw}\rho_0 c_{p0}\varepsilon_{tg}}{8}\left\{\frac{[(T_1(t) - \theta_1(t, z_{cw})]^2}{273.15 + T_1(t)} - 0.30\frac{[(T_1(0) - \theta_1(0, z_{cw})]^2}{273.15 + T_1(0)}\right\} \quad (15)$$

Implicit in Equation (15) is a constant in-plant power consumption corresponding to 30% of the gross electrical power based on initial tropical temperature conditions (second term between brackets). Such large parasitic losses result from a high flow rate intensity of about 7.5 m^3/s per net (design) megawatt. OTEC net power density as a function of cold seawater flow rate per unit area is the main focus of this large-scale study, i.e. P_{net}/A versus Q_{cw}/A.

Results and Discussion

The implementation of the model described in the previous Section was performed to estimate Atlantic OTEC resources when heat input from the atmosphere is either constant or changing with time. In the latter case, the polar relaxation temperatures τ_N and τ_S were allowed to increase for a while in order to simulate the potential effect of global warming with polar amplification (Lucarini and Stone, 2005a). Asymmetric scenarios with $\tau_N > \tau_S$ were preferentially considered since they promote the destabilization of the present-day THC.

Numerical Solution Procedure

Table 1 lists values of the parameters and initial conditions used in this work. As much as possible, this input is consistent with the work of Lucarini and Stone (2005a). For the tropical water-column temperature profiles, the following initial condition was adopted:

$$\theta_i(0,z) = T_S(0) + \{T_i(0) - T_S(0)\}\exp\{w(0)\frac{z-(h-h_m)}{K}\} \qquad \text{i} = 1, 2 \qquad (16)$$

A similar equation was used for salinity profiles. The turbulent vertical diffusion coefficient K was determined from imposing the condition $T_1(0)$- $\theta_1(0, z_{cw}) = 20°C$ for $z_{cw} = 4000$ m in Equation (16). In other words, the initial available OTEC temperature difference was fixed at 20°C for a selected deep seawater withdrawal depth of 1000 m. The value $K = 8540$ m^2/yr thus obtained is relatively high since $w(0) = 11.5$ m/yr; it reflects the need to balance strong upward advection of heat and salt with sufficient downward diffusive fluxes (at equilibrium). The OTEC mixed-effluent discharge location $z_{mix} = 4724$ m was determined by choosing initial neutral buoyancy.

The solution of partial differential Equations (9), (10) and (11) for the tropical water columns was accomplished by spatially discretizing the three domains $0 < z < z_{cw}$, $z_{cw} < z < z_{mix}$ and $z_{mix} < z < h - h_m$, as outlined in Nihous (2007). Equations (1) through (6) for the high-latitude boxes and tropical mixed layers were then added to the resulting set of ordinary differential equations. Convergence is controlled by diffusion in the deep-ocean equations, with the approximate condition $2K\delta t/(\delta z)^2 < 1$ (Nihous, 2007). This criterion was definitely satisfied with δz a little over 3 m and a time increment δt of about 3.5 hours. Comparing asymptotic results with known steady-state values, an accuracy of less than 1% was obtained. Although the overall solution procedure involved a total of nearly 6000 variables for the selected vertical resolution, computing times on a standard desktop computer (1.7 GHz, 1 GB RAM) were only of the order of 1.5 hour for simulations spanning 4000 years with over 10 million time steps. Because the THC equations are quite sensitive, the initial time $t = 0$ was defined after solving the system of equations for a simulated spin-up period of 1000 years. This ensured that a stable equilibrium had been reached before OTEC and global-warming scenarios were initiated.

Atlantic OTEC Resources without Global Warming

Before solving the model equations proposed in this study, the algorithm of Nihous (2005) was used with consistent input parameters to estimate steady-state Atlantic OTEC resources if advection $w(0)$ remained constant. Results are shown in Figure 2 as 'Atlantic 1-D'; also displayed are 'Overall 1-D' values for previously published worldwide estimates, over an area of 100 million km^2 (Nihous, 2005). The ordinate is P_{net}/A from Equation (15), while the

abscissa is proportional to Q_{cw}/A: the available (or zero-flow) net power is defined by setting $T_1(t) = T_1(0)$ and $\theta_1(t, z_{cw}) = \theta_1(0, z_{cw})$ in Equation (15). The strength of the Atlantic THC and the corresponding value $w(0)$ = 11.5 m/yr, instead of 4 m/yr in the worldwide analysis, allows greater OTEC flows before the thermal structure of the water column is affected. Thus, a maximum OTEC net power density of 83 kW/km^2 can be achieved in the Atlantic instead of 27 kW/km^2 'globally'. Given the area A of the Atlantic OTEC tropical sub-domain, this would amount to a total of 1.8 TW.

OTEC seawater flow rates corresponding to the steady-state maximum and $w = w(0)$ are considerable, however, and are of the same order of magnitude as $\widetilde{q}(0)$, with Q_{cw} = 9.4 Sv and Q_{ww} = 18.9 Sv. It is legitimate to wonder, then, how the THC could be affected by OTEC operations of such magnitude. In the present model, OTEC flows and the THC are coupled since $\widetilde{q}$ (i.e. w) is dynamically determined. A maximum disruption of the THC should be expected if OTEC flows were started impulsively at t = 0. Although they have no practical significance, impulsively-started OTEC operations for Q_{cw}/A = 3.75, 14 or 28 m/yr were selected to test the dynamical 'stiffness' of the model. Asymptotic values for these runs are displayed as dark squares in Figure 2. It is clear that large OTEC flows have no significant long-term impact on the THC. Figure 3 shows the time course of THC strength; oscillations of $\widetilde{q}$ remain within 1 Sv and are damped within 500 years. As long as the background THC is strong enough (e.g. 15.6 Sv at its present-day value), large OTEC flows will not significantly disturb it. The cause for such system stiffness, within the confines of this simple model, probably lies in the fact that OTEC flows sum up to zero through the water column since effluent discharge exactly matches deep and surface seawater intakes.

OTEC net power density was then calculated for a more realistic OTEC implementation scenario corresponding to a linear buildup of OTEC operations, with Q_{cw}/A increasing from 0 to 14 m/yr over 1000 years. This would represent about 3.8 GW/year if OTEC flows did not affect the thermal structure of the tropical water column. The time series of actual net power density is shown later as a reference in the context of global warming.

Note that the present approach does not allow for possible adaptive strategies since most OTEC operational parameters are fixed. It could be argued, for example, that extending the cold seawater intake to greater depths could minimize or offset any reduction in the initial OTEC temperature differential as needed. The asymptotic temperature profile (t = 3000 years) corresponding to the previous increase of Q_{cw}/A from 0 to 14 m/yr over 1000 years shows a temperature difference of 20°C between the surface and a depth of 1300 m. A modification of ($h - z_{cw}$) from 1000 m to 1300 m would redefine the domains where Equations (9) and (10) are applicable, however, and the temperature profile would change further. For the example discussed above, the asymptotic actual net power density is 83 kW/km^2 when ($h - z_{cw}$) is equal to 1000 m (baseline), i.e. about half of the available net power density of 179 kW/km^2 based on an OTEC temperature difference of 20°C. Repeating calculations with ($h - z_{cw}$) equal to 1300 m yields an asymptotic actual net power density of 122 kW/km^2. This enhanced OTEC resource reflects better zero-flow OTEC conditions, rather than a reduction in the relative impact of OTEC flows, since seawater at a depth of 1300 m *initially* is 2.7°C colder. Any detailed assessment of adaptive strategies is left for the future.

Atlantic OTEC Resources with Global Warming

The potential development of large widespread OTEC operations over tropical oceans could not realistically take place over time scales smaller than centuries. This essentially would be a time frame of the same order as global warming. Simple global warming scenarios were defined in Lucarini and Stone (2005a), and their approach will be followed here. It consists in letting τ_N linearly increase from $\tau_N(0)$ to a selected value $\tau_N(0) + \Delta\tau_N$ over a period t_0. In order to mimic the polar amplification of expected global warming effects, tropical relaxation temperatures are not modified. The southern relaxation temperature τ_S is assumed to increase like τ_N, but only fractionally. This arbitrary choice reflects a desire to simulate worst-case scenarios where the present-day THC could be destabilized. A critical transition occurs when the THC reverses direction as $\tilde{q}$ changes sign[2]. As a caveat, it is noted here that a collapse (critical transition) of the THC is deemed a "low probability – high impact" risk associated with global warming (Rahmstorf, 2006). Therefore, a strong North-South warming asymmetry can be postulated *a priori* in our simplified model, but it would have to be justified *a posteriori* to lend credibility to model results. Recent OGCM predictions of surface temperatures under a wide range of greenhouse-gas emission scenarios were published by the Intergovernmental Panel on Climate Change (IPCC, 2007). They strongly suggest that a North-South warming asymmetry would persist through the forecast period (21st Century) and that substantial northern warming would take place even with t_0 as small as 100 years (cf. *Figure SPM-6* in reference).

Although the parametric effects of asymmetric polar warming and of warming duration are examined later, a baseline case initially is defined by $\Delta\tau_S = 0.3\ \Delta\tau_N$ and $t_0 = 1000$ years. Note

[2] The physical significance of a reversed THC is not known. OGCM investigations of a shutdown of North Atlantic Deep Water formation indicate a significant cooling in northern high latitudes, a southward shift of the Inter Tropical Convergence Zone and a sea level rise of about 1 m in the North Atlantic (Rahmstorf, 2006).

that the 'warm-ocean' scenario discussed in Nihous (2005) is probably unrealistic; a warmer tropical mixed layer was allowed while keeping the input polar seawater temperature constant; even though a downward adjustment of w was provided, this 'warm ocean' would correspond to a *tropical amplification* of global warming.

First, the effect of model architecture is assessed since the tropical water column is vertically resolved here while the tropical ocean is a well-mixed box in Lucarini and Stone (2005a). Comparing Figure 4 and the results of Lucarini and Stone (2005a, *Figure 7*), it appears that the critical transition corresponds to values of $\Delta\tau_N$ about 1°C higher, between 7.35°C and 7.5°C, when advection and diffusion are incorporated in a tropical water column. Results are otherwise consistent: a weakened subcritical THC oscillates while a supercritical THC settles to a stronger circulation than the present-day THC. A dramatic change in *available* OTEC net power density takes place for these global warming scenarios. The ordinate in Figure 5 is the ratio of the temperature dependent bracket in Equation (15) for the selected global warming scenario over the same bracket under present-day conditions. In both subcritical and supercritical cases, the available OTEC resource is degraded but in the latter case, it somewhat recovers following the THC reversal. Since the *actual* OTEC net power density benefits from high advection rates w, it can be anticipated that because of the stronger reverse THC in supercritical scenarios, actual OTEC operations could overcome the loss in available net power density. This, however, might take place after a very long time.

The stability analysis of the THC under global-warming forcings was repeated when large OTEC operations are also developed. The choice of Q_{cw}/A = 14 m/yr linearly implemented over 1000 years was chosen with little loss of generality; this value corresponds to the maximum actual net power density without global warming. Although large OTEC

operations do not affect a strong THC, they have the ability to enhance the destabilization of a weak one. This can be seen in Figure 6 where the critical transition occurs for values of $\Delta\tau_N$ about 0.3°C lower with OTEC operations, between 7.0°C and 7.2°C. Figure 7 shows the corresponding time histories of actual net power density; the case without global warming also is displayed. Actual net power density here combines the effects of global warming (if any) and of OTEC flows upon the vertical thermal structure of the OTEC tropical sub-domain. In both subcritical and supercritical cases, OTEC resources disappear before the 'implementation period' of 1000 years is even completed. Only after another thousand years or so, when the THC reversal takes place for the supercritical scenario, substantial stable OTEC resources 'reappear' and even exceed those with $\Delta\tau_N = 0$. This shows that in the case under consideration, the benefit of a very strong reverse THC outweighs the loss of available net power density. For the sake of completeness, the steady-state algorithm with fixed advection rate w (Nihous, 2005) corresponding to the reverse THC in Figure 5 ($\Delta\tau_N = 7.5$°C) was used to evaluate 'supercritical steady-state OTEC resources'. The result is shown in Figure 2.

Finally, the parametric effects of the polar asymmetry and duration of global warming were examined for a fixed value $\Delta\tau_N = 7.0$°C and OTEC flows corresponding to $Q_{cw}/A = 14$ m/yr linearly implemented over t_0 years. Recall that with the earlier warming 'baseline' ($t_0 = 1000$ years; $\Delta\tau_S = 0.3\Delta\tau_N$), these choices of $\Delta\tau_N$ and OTEC flows correspond to the subcritical case in Figures 6 and 7. Figure 8 shows the effect of asymmetric polar warming on actual OTEC net power density when $t_0 = 1000$ years. Since the most asymmetric case is subcritical, all cases are subcritical as well. The THC is weaker when southern warming is relatively smaller (more asymmetric). In the symmetric case $\Delta\tau_S = \Delta\tau_N$, the THC asymptotically settles

to a slightly larger value than initially, at 17.5 Sv. Yet, this relative benefit is now offset with a large southern polar warming of 7.0°C and the combined effect remains rather detrimental: asymptotic actual net power density hardly exceeds 30 kW/km^2. Note that for all warming cases illustrated in Figure 8, an asymptotic temperature difference of 20°C is found between the surface and greater water depths, between 2100 m and 2300 m. This would make the withdrawal of deeper cold seawater a much more difficult adaptive strategy to implement. Figure 9 is similar to Figure 8 with t_0 = 200 years. The work of Lucarini and Stone (2005a) generally shows that, all other things being equal, the THC is more susceptible to destabilization with a more abrupt warming, and that this effect is more pronounced under more asymmetric polar warming. This behavior has dramatic consequences for $\Delta\tau_S = 0.3\Delta\tau_N$ with the THC rapidly reversing; in other words, shortening t_0 in this case induces a critical THC transition soon enough to boost the actual OTEC net power density above its no-warming levels without a previous collapse. Of the simplified global warming scenarios investigated in this study, this rapid asymmetric case is the only one for which OTEC operations might not be severely hampered or could even improve in the relatively short term (within the limits of our modeling). Without a critical transition, however, shortening t_0 does not affect asymptotic values of actual net power density but it significantly worsens the situation in the transitional OTEC implementation period.

Conclusions

Since OTEC is based on utilizing the oceanic vertical thermal structure and that only about half of the tropical waters of the Atlantic are suitable for OTEC operations, a published interhemispheric three-box model of the Atlantic THC (Lucarini and Stone, 2005a) was modified by replacing the single tropical box with two vertically-resolved advection-

diffusion one-dimensional sub-domains. Seawater flows from large-scale OTEC were then allowed in one of the tropical sub-domains. Under present conditions, calculations showed that steady-state OTEC net power production density would reach a maximum of about 80 kW/km^2 (corresponding to 1.8 TW) with a cold seawater flow per unit area of about 14 m/yr (corresponding to 9.4 Sv). This maximum reflects the impact of large OTEC flows on the oceanic thermal structure within the OTEC sub-domain as a disruption of advective upward fluxes takes place above the OTEC cold seawater intake depth. The Atlantic OTEC power density maximum is larger than a recently suggested worldwide value of the order of 30 kW/ km^2 (Nihous, 2005) because of the relative strength of the Atlantic THC. Large OTEC operations were found to have minimal effects on the overall THC strength, at its present value of 15.6 Sv.

Under scenarios of asymmetric high-latitude warming over 1000 years potentially representative of current global warming trends, the available (zero-flow) OTEC temperature difference decreased. For a high subcritical case and OTEC flows corresponding to the present-day steady-state maximum, it was shown that no OTEC net power would be recoverable after about 1300 years, although the relative loss would have started many centuries earlier. For a marginally supercritical case and the same OTEC flows, matters would not be very different until the THC reversal takes place, after more than 2000 years. The emergence of this stronger THC, at about 40 Sv, would enhance vertical advection in the tropical sub-domains and eventually boost recoverable OTEC resources to about twice their present-day steady-state maximum, i.e. to a net power density of nearly 170 kW/km^2 (3.6 TW), in spite of less favorable OTEC temperature differences. Finally, the parametric effects of warming duration and polar asymmetry were investigated. It appeared that as long as the THC does not reverse direction (subcritical cases), more symmetric warming scenarios and

longer warming periods were relatively favorable, although actual OTEC net power density would always be well below comparable no-warming levels. For a more abrupt, asymmetric warming scenario over 200 years, it was demonstrated that a THC reversal might occur rapidly enough to prevent a collapse of OTEC resources during the critical transition; instead, the asymptotic enhancement of OTEC net power density resulting from a strong reverse THC could occur while the OTEC technology is being implemented.

Such events remain highly hypothetical and would unfold over centuries. The mere possibility of their occurrence, however, challenges the accepted notion that OTEC resources are forever renewable. The present results certainly should not be viewed as a reason against developing OTEC resources, but rather as an example of the profound environmental changes that could be caused by global warming. While further modeling efforts are under way, the question of quantifying OTEC resources with or without global warming should eventually be addressed with Ocean General Circulation Models.

Nomenclature

A	surface area of model box or sub-domain (m^2)
c_{p0}	average specific heat of seawater (J/kg-K)
$\widetilde{F}$	freshwater flux from atmosphere into high-latitude boxes and tropical mixed layers (m^3/s)
h	ocean depth (m)
h_m	tropical mixed layer thickness (m)
$\widetilde{H}$	heat flux from atmosphere into high-latitude boxes and tropical mixed layers (W)
k	THC hydraulic constant (s^{-1})
K	vertical eddy diffusion coefficient in tropical water columns (m^2/s)
P_{net}	OTEC net power (W)
$\widetilde{q}$	algebraic strength of the THC (m^3/s)
Q_{cw}	OTEC cold seawater flow rate (m^3/s)
Q_{ww}	OTEC warm seawater flow rate (m^3/s)
s	salinity in advective-diffusive tropical water columns (psu)
S	salinity in high-latitude boxes and tropical mixed layers (psu)
t	time (s)
t_0	duration of global warming period (s)
T	temperature in high-latitude boxes and tropical mixed layers (°C)
V	volume of model box or sub-domain (m^3)
w	upwelling rate in advective-diffusive tropical water columns (m/s)
z	vertical coordinate measured from the seafloor (m)
z_{cw}	vertical coordinate of OTEC cold seawater intake (m)

z_{mix} vertical coordinate of OTEC mixed effluent discharge (m)

Greek letters

α seawater thermal expansion coefficient ($°C^{-1}$)

β seawater haline expansion coefficient (psu^{-1})

δt time step in numerical calculations (s)

δz vertical mesh size in numerical calculations (m)

$\Delta\tau$ maximum increase of polar relaxation temperature from global warming (°C)

γ ratio of OTEC seawater flow rates Q_{ww}/Q_{cw}

ε_{tg} turbogenerator efficiency

λ thermal relaxation coefficient (s^{-1})

ρ_0 average seawater density (kg/m^3)

θ temperature in advective-diffusive tropical water columns (°C)

τ thermal relaxation target temperature (°C)

Indices

1 tropical sub-domain where OTEC operations are allowed

2 tropical sub-domain where OTEC operations are not allowed

N Northern high-latitude box

S Southern high-latitude box

REFERENCES

d'Arsonval, A., 1881. Utilisation des forces naturelles. Avenir de l'électricité. Revue Scientifique, 17, 370-372.

Avery, W. H. and C. Wu, 1994. Renewable Energy from the Ocean – A Guide to OTEC. In: Johns Hopkins University Applied Physics Laboratory Series in Science and Engineering, J.R. Apel ed., Oxford University Press, New York.

Broecker, W. S., 1997. Thermohaline Circulation, the Achilles Heel of Our Climate system: Will Man-Made CO_2 Upset the Current Balance. Science, 278(5343), 1582-1588.

Claude, G., 1930. Power from the Tropical Seas. Mechanical Engineering, 52(12), 1039-1044.

Intergovernmental Panel on Climate Change (IPCC), 2007. Climate Change 2007: The Physical Science Basis – Summary for Policymakers. United Nations Environment Programme (UNEP) and World Meteorological Organization (WMO) publication, http://www.ipcc.ch/SPM2feb07.pdf, 18 pp.

Johnson, F. A., 1992. Chapter 5: Closed-Cycle Ocean Thermal Energy Conversion. In: Ocean Energy Recovery – The State of the Art, R. J. Seymour ed., ASCE pub., New York, 70-96.

Lucarini, V and P. H. Stone, 2005a. Thermohaline Circulation Stability: A Box Model Study. Part I: Uncoupled Model. Journal of Climate, 18, 501-513.

Lucarini, V and P. H. Stone, 2005b. Thermohaline Circulation Stability: A Box Model Study. Part II: Coupled Model. Journal of Climate, 18, 514-529.

Lucarini, V., S. Calmanti and V. Artale, 2005. Destabilization of the thermohaline circulation by transient changes in the hydrological cycle. Climate Dynamics, 24, 253-262.

Marotzke, J., 2000. Abrupt climate change and thermohaline circulation: Mechanisms and predictability. Proceedings of the National Academy of Sciences, 97(4), 1347-1350.

Masutani, S. M. and P. K. Takahashi, 2000. Ocean Thermal Energy Conversion. In: Encyclopedia of Electrical and Electronics Engineering, Vol. 15, J. G. Webster ed., John Wiley & Sons, New York, 93-103.

Nihous, G. C., 2005. An order-of-magnitude estimate of Ocean Thermal Energy Conversion (OTEC) resources. Journal of Energy Resources and Technology, 127(4), 328-333.

Nihous, G. C., 2007. A preliminary assessment of Ocean Thermal Energy Conversion (OTEC) resources. Journal of Energy Resources and Technology, 129(1), 10-17.

Penney, T. R. and D. Bharathan, 1987. Power from the Sea. Scientific American, 256, 86-92.

Penney, T. R. and T. H. Daniel, 1989. Energy from the ocean: a resource for the future. Year Book for 1989, Encyclopædia Britannica, 98-115.

Rahmstorf, S., M. Crucifix, A. Ganopolsky, H. Goosse, I. Kamenkovich, R. Knutti, G. Lohmann, R. Marsh, L. A. Mysak, Z. Wang and A. J. Weaver, 2005. Thermohaline circulation hysteresis: A model intercomparison. Geophysical Research Letters, 32, L23605, 5 pp.

Rahmstorf, S., 2006. Thermohaline Ocean Circulation. In: Encyclopedia of Quaternary Sciences, S. A. Elias ed., Elsevier, Amsterdam, 10 pp.

Rooth, C., 1982. Hydrology and ocean circulation. Progress in Oceanography, 11, 131-149.

Stocker, T. F. and A. Schmittner, 1997. Influence of CO_2 emission rates on the stability of the thermohaline circulation. Nature, 388, 862-865.

Stommel, H., 1961. Thermohaline convection with two stable regimes. Tellus, 13, 224-230.

Vega, L. A., 1995. Ocean Thermal Energy Conversion. In: Encyclopedia of Energy Technology and the Environment, Vol. 3, A. Bisio and S. Boots eds., John Wiley & Sons, New York, 2104-2119.

Zener, C., 1973. Solar Sea Power. Physics Today, 26, 48-53.

Zener, C., 1977. The OTEC Answer to OPEC: Solar Sea Power. Mechanical Engineering, 99(12), 26-29.

LIST OF FIGURE CAPTIONS

Figure 1 – Schematic model of the thermohaline circulation ($\widetilde{q} > 0$)

Figure 2 – Actual and available (zero flow) steady-state OTEC net power density.

Figure 3 – THC strength following an abrupt (stepwise) implementation of OTEC operations.

Figure 4 – Critical transition of the THC for asymmetric high-latitude warming scenarios (t_0 = 1000 years; $\Delta\tau_S = 0.3\Delta\tau_N$).

Figure 5 – Relative change in available OTEC net power density for subcritical and supercritical asymmetric high-latitude warming scenarios (t_0 = 1000 years; $\Delta\tau_S = 0.3\Delta\tau_N$).

Figure 6 – Critical transition of the THC for asymmetric high-latitude warming scenarios (t_0 = 1000 years; $\Delta\tau_S = 0.3\Delta\tau_N$) and OTEC cold seawater flows per unit area increasing from 0 to 14 m/yr over 1000 years.

Figure 7 – Actual OTEC net power density for asymmetric high-latitude warming scenarios (t_0 = 1000 years; $\Delta\tau_S = 0.3\Delta\tau_N$) and OTEC cold seawater flow per unit area increasing from 0 to 14 m/yr over 1000 years.

Figure 8 – Actual OTEC net power density for high-latitude warming scenarios of varying asymmetry (t_0 = 1000 years; $\Delta\tau_N$ = 7.0°C) and OTEC cold seawater flow per unit area increasing from 0 to 14 m/yr over 1000 years.

Figure 9 – Actual OTEC net power density for high-latitude warming scenarios of varying asymmetry (t_0 = 200 years; $\Delta\tau_N$ = 7.0°C) and OTEC cold seawater flow per unit area increasing from 0 to 14 m/yr over 1000 years.

Table 1 – Selected model values

Parameters		footnote	Initial		footnote
A	21.3 x 10^6 km^2	[1]	$T_N(0)$	2.9 °C	[3]
c_{p0}	4 kJ/kg-K	[2]	$T_S(0)$	0.3 °C	[3]
$\widetilde{F}_N$	0.41 Sv	[3]	$T_i(0)$ i =1, 2	28.4 °C	[3]
$\widetilde{F}_S$	0.27 Sv	[3]	$S_N(0)$	34.7 psu	[3]
h	5000 m	[3]	$S_S(0)$	34.1 psu	[3]
h_m	75 m	[2]	$S_i(0)$ i =1, 2	35.6 psu	[3]
k	1.5 x 10^{-6} s^{-1}	[3]	$\widetilde{q}(0)$	15.6 Sv	[7]
K	8540 m^2/yr	[4]			
z_{cw}	4000 m	[5]			
z_{mix}	4724 m	[6]			
α	1.5 x 10^{-4} $°C^{-1}$	[3]			
β	8 x 10^{-4} psu^{-1}	[3]			
γ	2	[2]			
ε_{tg}	0.85	[2]			
λ	1.29 x 10^{-9} s^{-1}	[3]			
ρ_0	1025 kg/m^3	[2]			
τ_i i = N, S	0 °C	[3]			
τ_i i = 1, 2	30 °C	[3]			

[1] 1/24 of Earth surface (sphere of average radius 6378.135 km)
[2] Nihous (2005)
[3] Lucarini and Stone (2005a)
[4] adjusted to yield an initial temperature of 8.4 °C at a depth of 1000 m
[5] OTEC cold water intake depth of 1000 m
[6] coordinate where initial OTEC effluent discharge is neutrally buoyant
[7] value after numerical spin-up of 1000 years

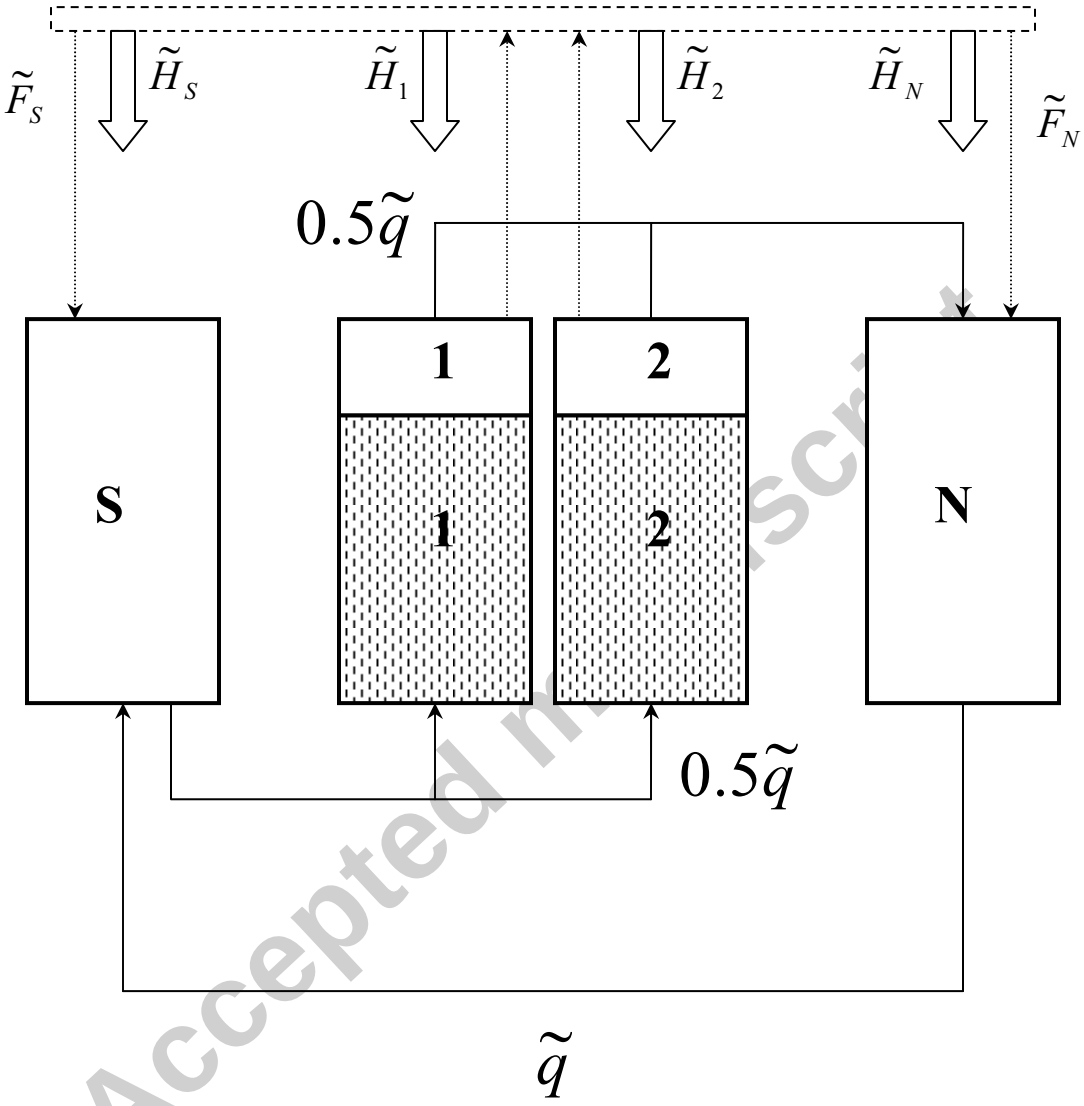

Figure 1 – Schematic model of the thermohaline circulation ($\tilde{q} > 0$)

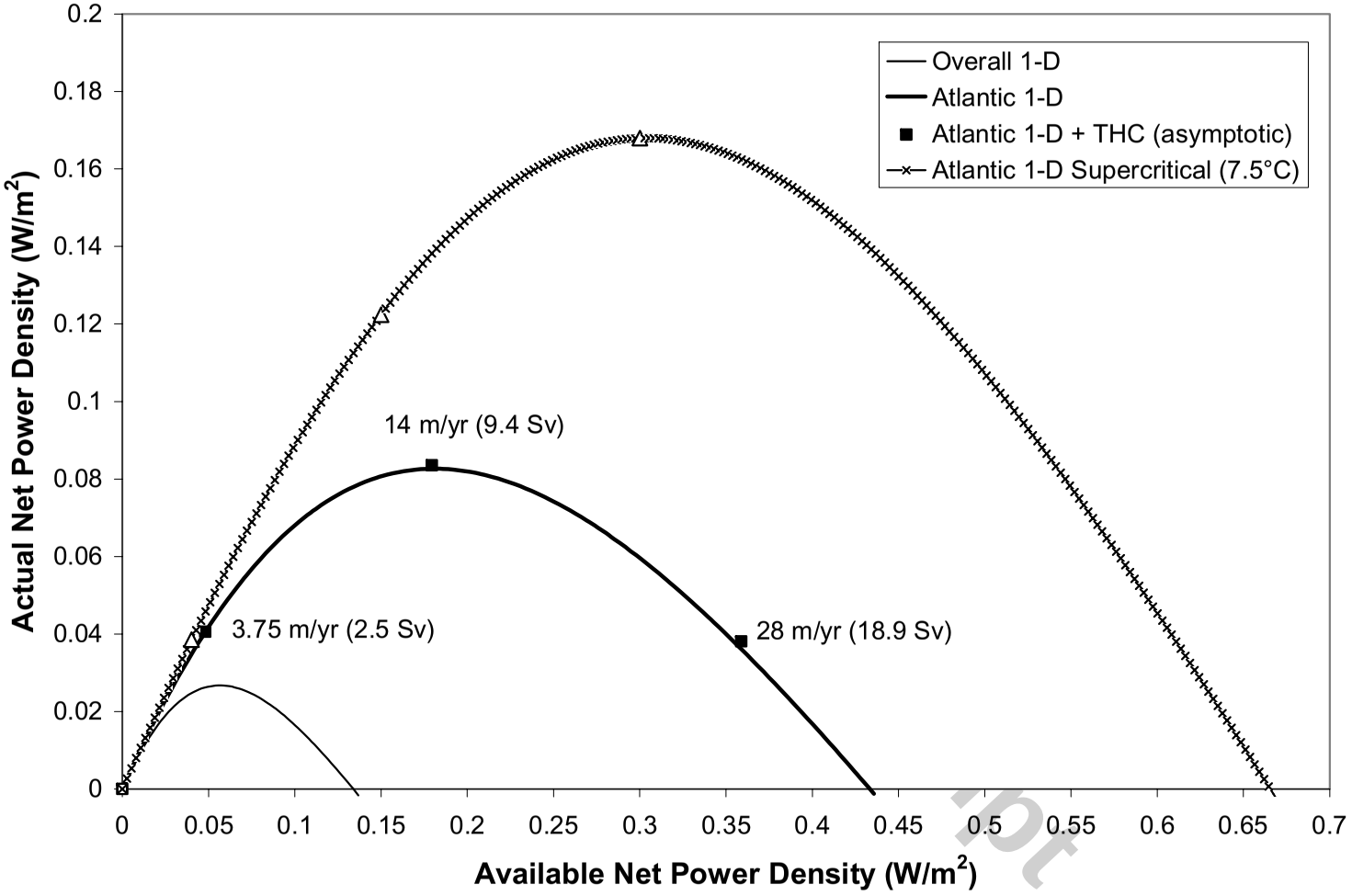

Figure 2 – Actual and available (zero flow) steady-state OTEC net power density.

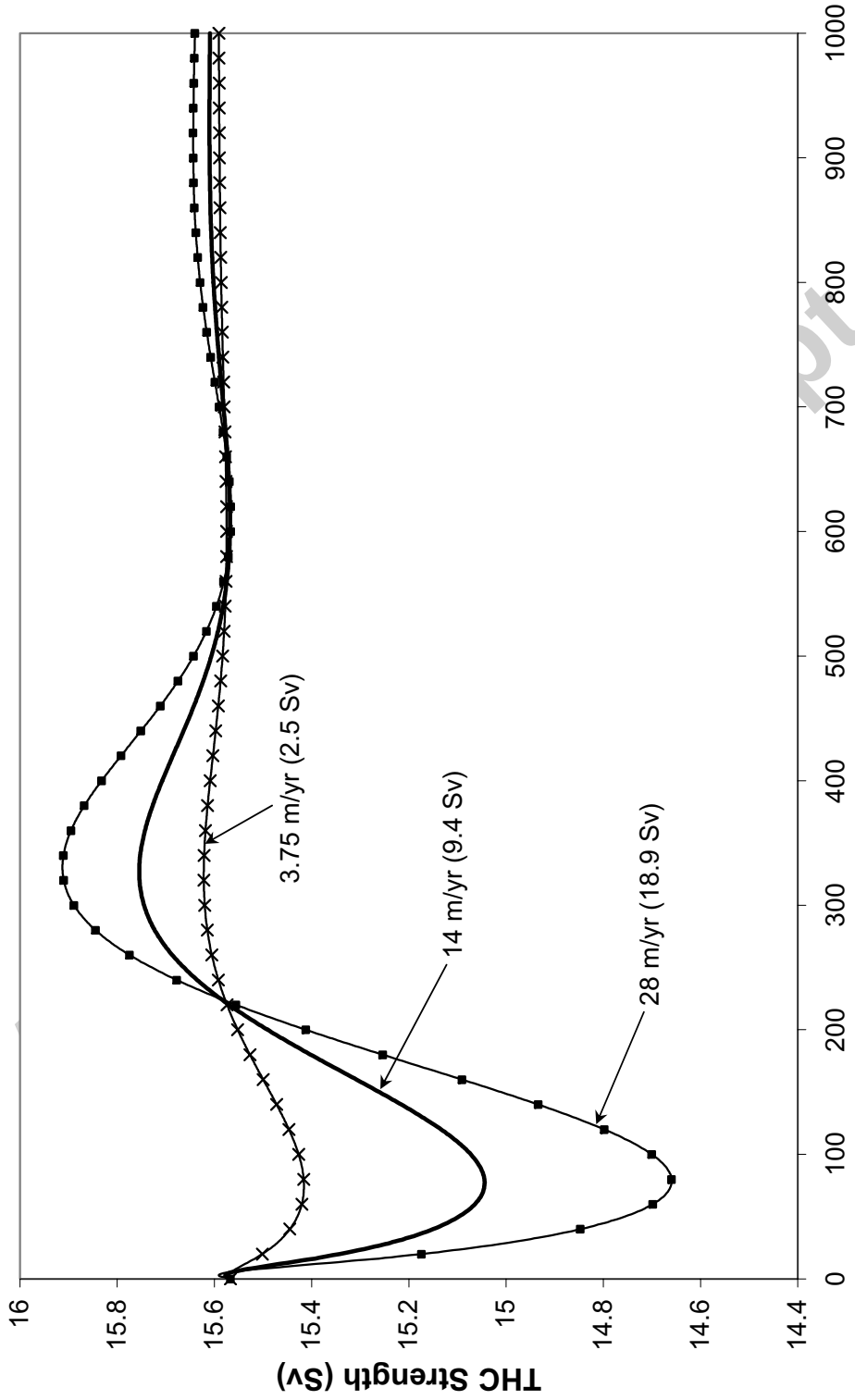

Figure 3 – THC strength following an abrupt (stepwise) implementation of OTEC operations.

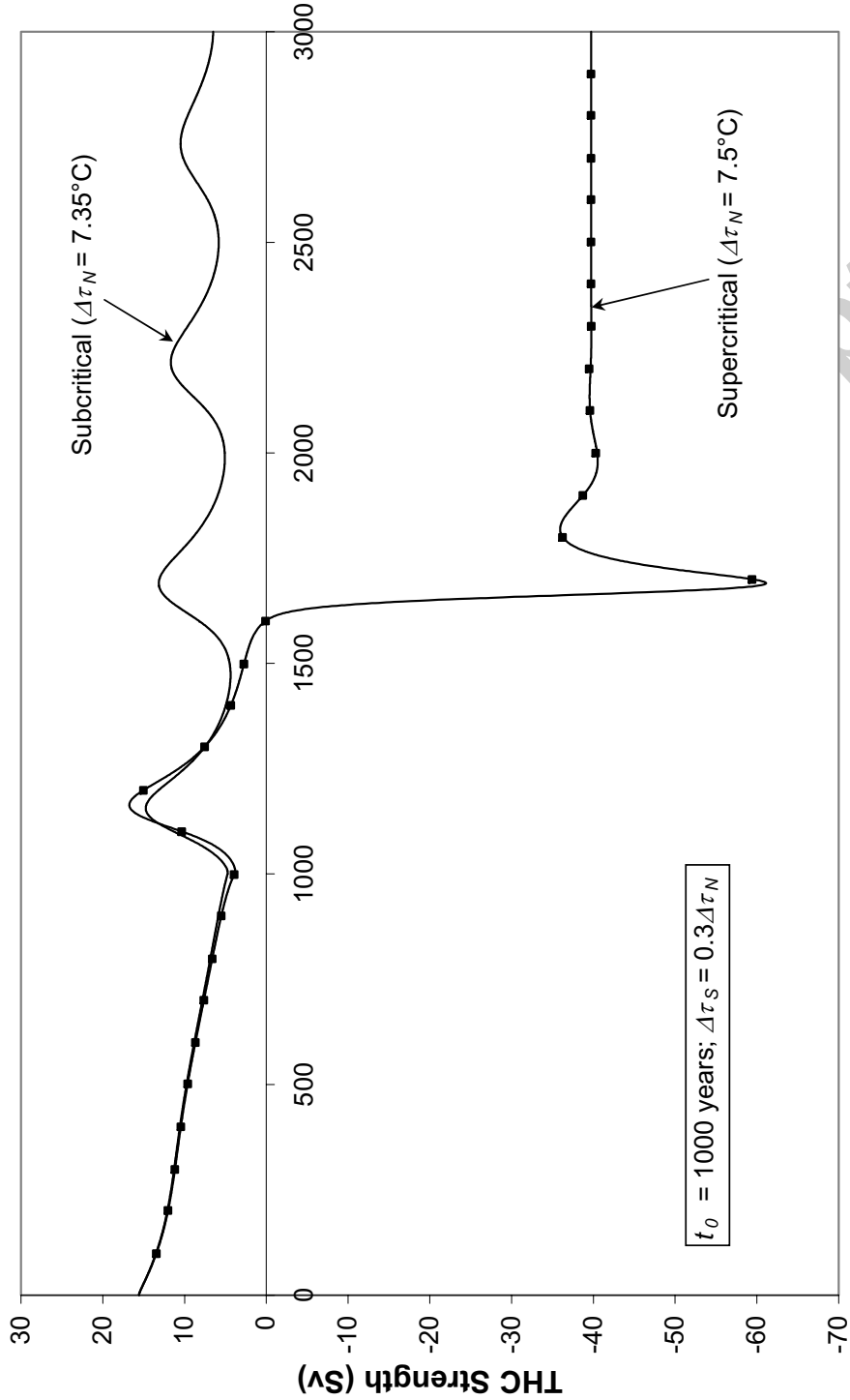

Figure 4 – Critical transition of the THC for asymmetric high-latitude warming scenarios (t_0 = 1000 years; $\Delta\tau_S = 0.3\Delta\tau_N$).

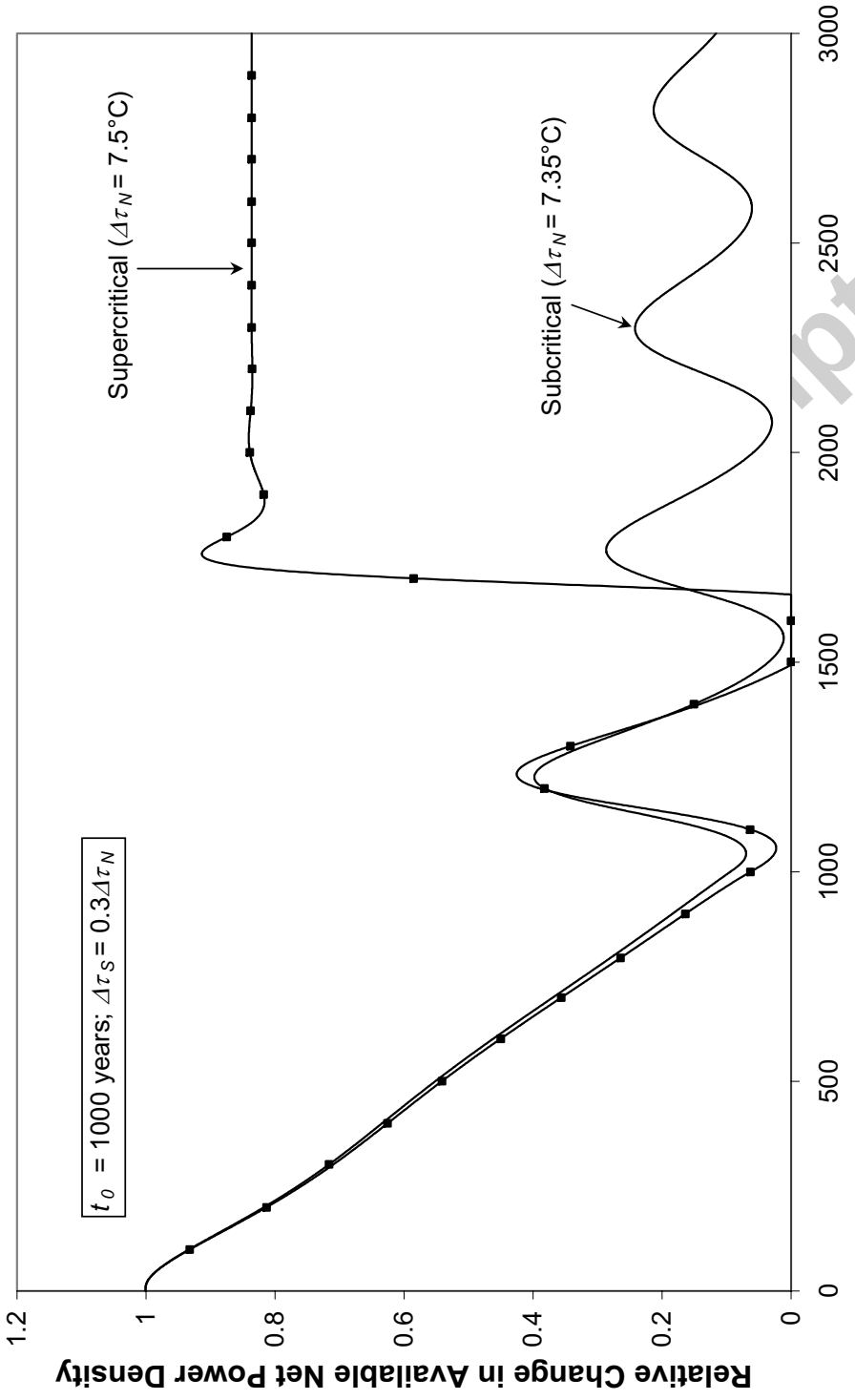

Figure 5 – Relative change in available OTEC net power density for asymmetric high-latitude warming scenarios (t_0 = 1000 years; $\Delta\tau_S = 0.3\Delta\tau_N$).

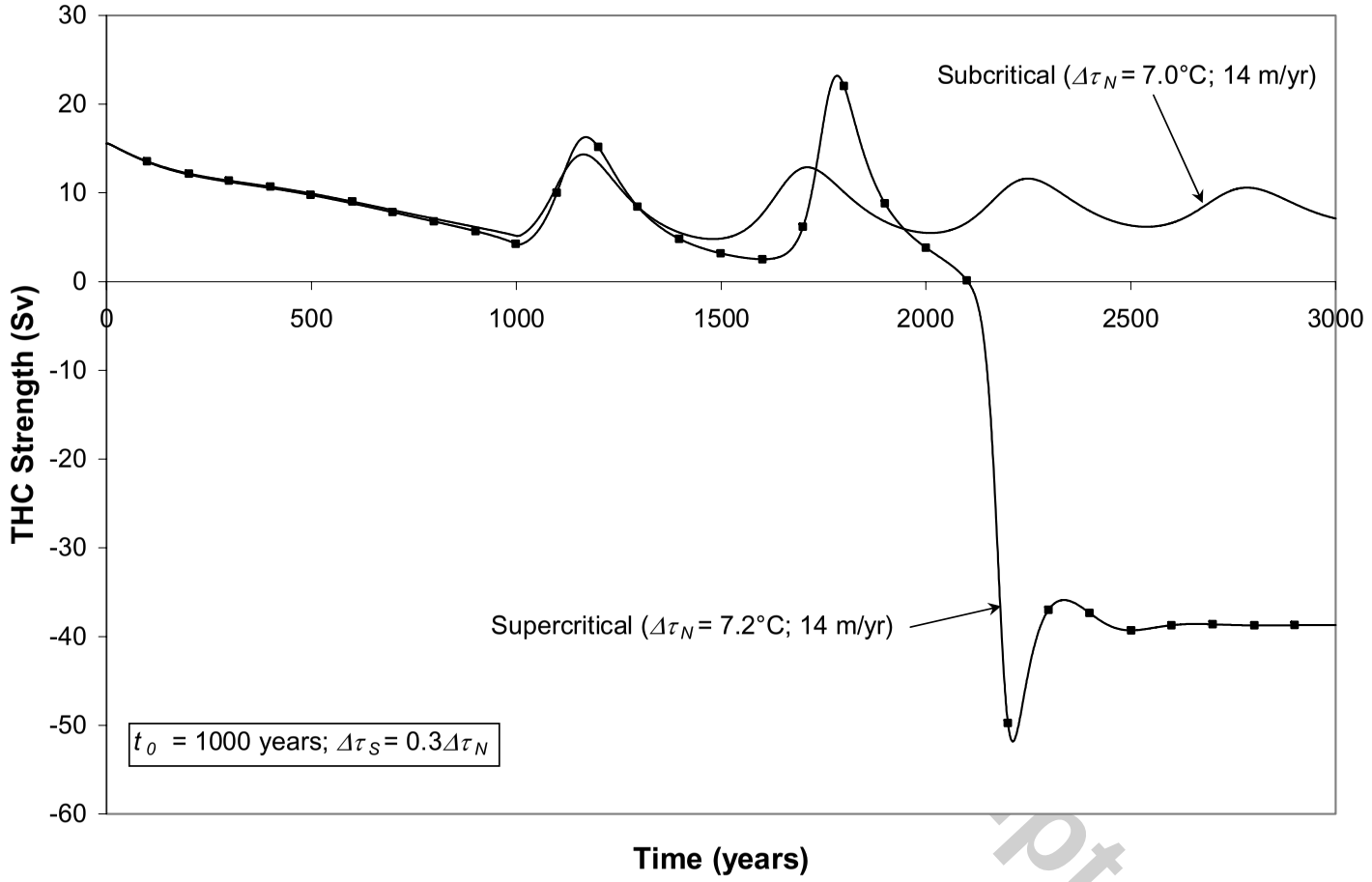

Figure 6 – Critical transition of the THC for asymmetric high-latitude warming scenarios (t_0 = 1000 years; $\Delta\tau_S = 0.3\Delta\tau_N$) and OTEC cold seawater flow per unit area increasing from 0 to 14 m/yr over 1000 years.

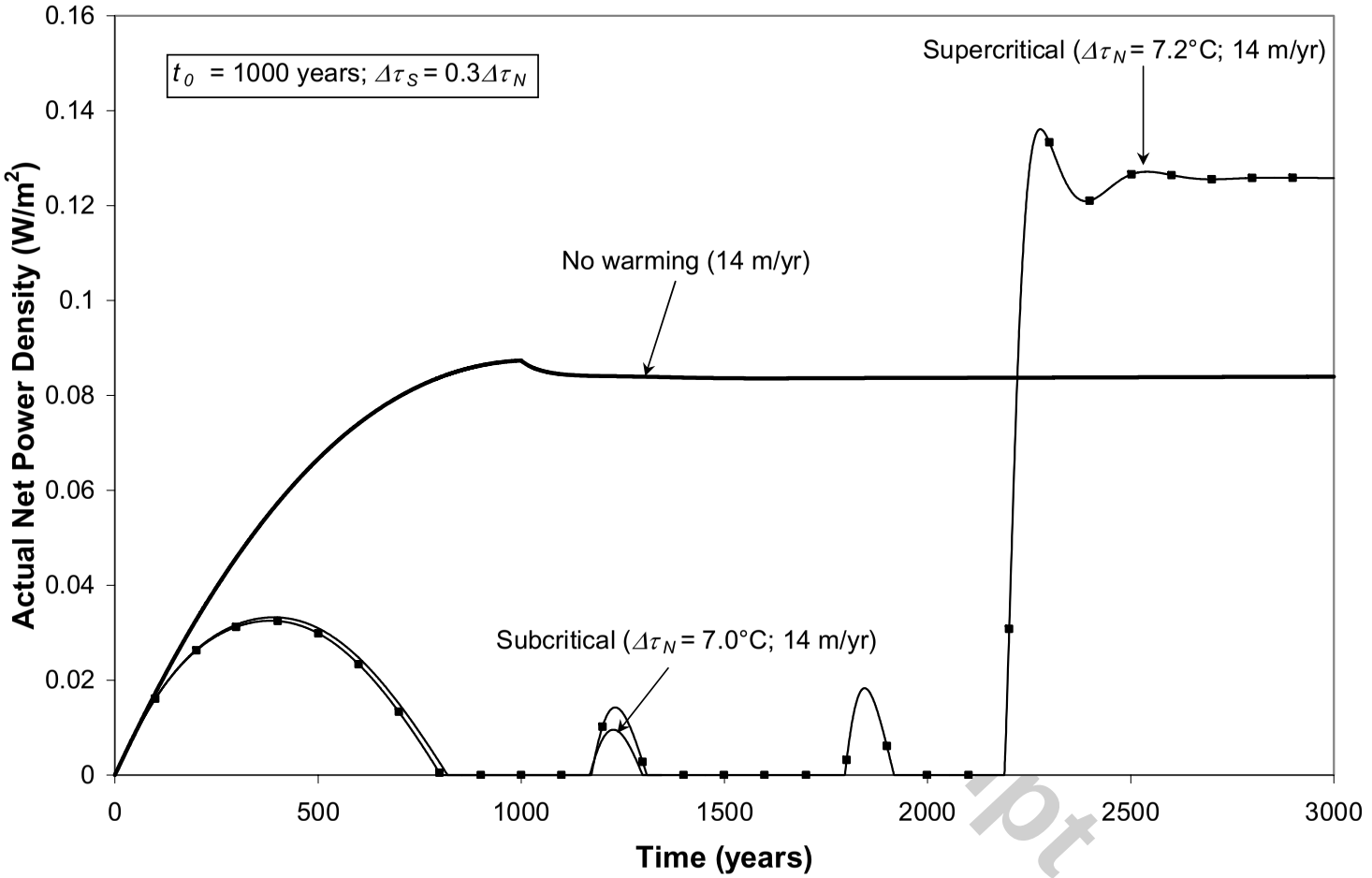

Figure 7 – Actual OTEC net power density for asymmetric high-latitude warming scenarios (t_0 = 1000 years; $\Delta\tau_S = 0.3\Delta\tau_N$) and OTEC cold seawater flow per unit area increasing from 0 to 14 m/yr over 1000 years.

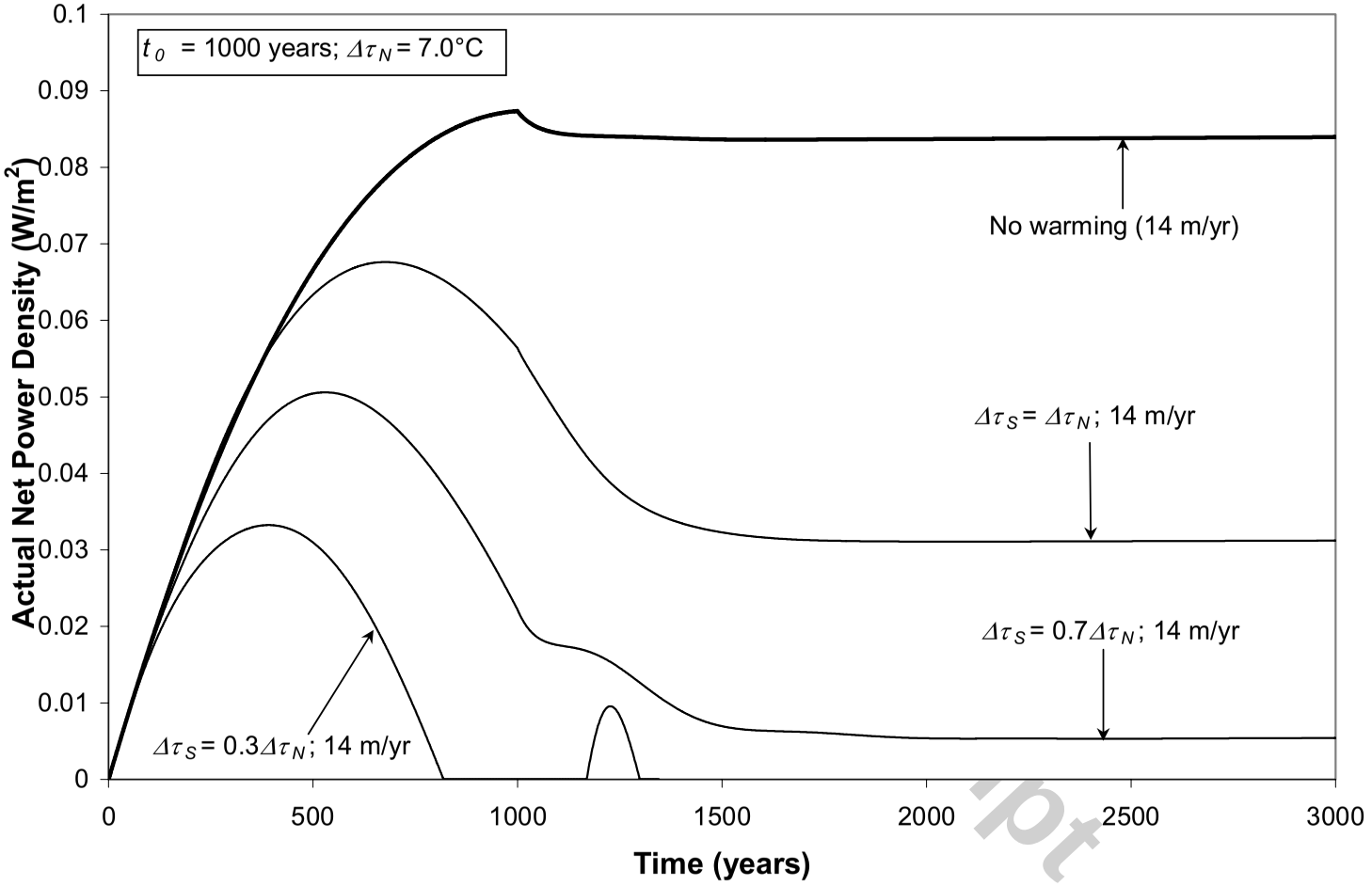

Figure 8 – Actual OTEC net power density for high-latitude warming scenarios of varying asymmetry (t_0 = 1000 years; $\Delta\tau_N$ = 7.0°C) and OTEC cold seawater flow per unit area increasing from 0 to 14 m/yr over 1000 years.

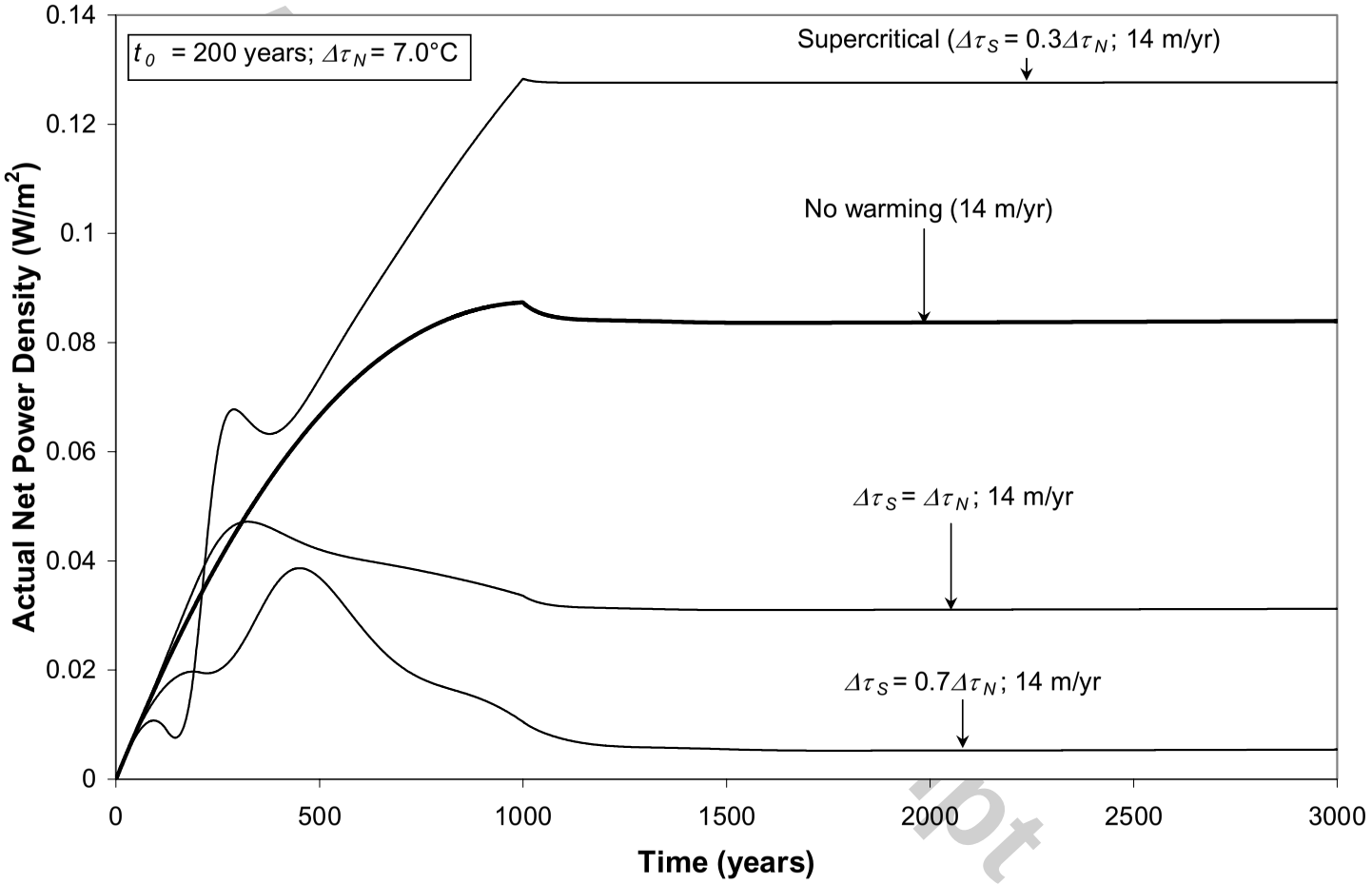

Figure 9 – Actual OTEC net power density for high-latitude warming scenarios of varying asymmetry (t_0 = 200 years; $\Delta\tau_N$ = 7.0°C) and OTEC cold seawater flow per unit area increasing from 0 to 14 m/yr over 1000 years.